Rapid and facile fabrication of hierarchically porous graphene aerogel for oil-water separation and piezoresistive sensing applications

[$]Yirui Mu[1], [$]Lin Wang[2], Rui Zhang*[3], Rami Adel Pashameah[4], Eman Alzahrani[5], Zhengzheng Li[1], Abdullah K. Alanazi[5], Hassan Algadi[6], Mina Huang[7], Zhanhu Guo[8,9], Tong Wan*[1] ·Huige Wei*[1]

[1] Tianjin Key Laboratory of Brine Chemical Engineering and Resource Eco-utilization, College of Chemical Engineering and Materials Science, Tianjin University of Science and Technology, Tianjin, 300457, China

[2] GRINM Group Co., Ltd., Beijing 100088, China (wanglin@grinm.com)

[3] College of Mechanical Engineering, Tianjin University of Science and Technology, Tianjin, 300457, China

[4] Department of Chemistry, Faculty of Applied Science, Umm Al-Qura University, Makkah 24230, Saudi Arabia

[5] Department of Chemistry, College of Science, Taif University, Taif 21944, Saudi Arabia

[6] Department of Electrical Engineering, Faculty of Engineering, Najran University, Najran, 11001, Kingdom of Saudi Arabia

[7] College of Materials Science and Engineering, Taiyuan University of Science and Technology, Taiyuan, 030024, China

[8] Department of Chemical and Bimolecular Engineering, University of Tennessee, Knoxville, TN, 37996, USA

9 Integrated Composites Lab, Department of Mechanical and Construction Engineering, Northumbria University, Newcastle Upon Tyne, NE1 8ST, UK

$ These authors contribute equally to this work.

*E-mail: zhangrui19850424@tust.edu.cn;
*E-mail: wantong@tust.edu.cn;
*E-mail: huigewei@tust.edu.cn

ABSTRACT

Graphene aerogel (GA) holds great potentials for versatile applications, for example, oil-water separation and piezoresistive sensing. However, GA is generally prepared via time-consuming and complicated methods. Herein, a rapid and facile approach has been proposed to fabricate GA by a two-step reduction method, i.e., hydrothermal reduction by thiourea at a mild temperature of 95 ^{o}C for 30 min followed by microwave treatment for several seconds, c.a., 6-14 s. GA was partially reduced in the first step and self-assembled into a 3D scaffold which is much more receptive to microwaves and promotes the second complete reduction by microwave treatment. By tuning the microwaving time, the GA microwaved for 10 s, that is, MGA-10 exhibits hierarchically porous microstructure, ultra-low density, and super compressibility. MGA-10 can be used as a recyclable absorbent with high absorption capacities (223~430 g/g) towards various oils and organic solvents. Meanwhile, the high sensitivity of the electric resistance to the compressive strain enables MGA-10 promising for pressure sensor applications. The MGA-10 sensor demonstrates high sensitivity (1.112 kPa^{-1} at a pressure range of 0~0.3 kPa) and excellent stability (> 3000 cycles). This fabrication route paves the way to efficiently prepare highly compressible graphene aerogels for versatile applications.

Keywords: Graphene aerogel; two-step reduction; microwave; oil-water separation; pressure sensor

1. Introduction

Graphene aerogel (GA), inheriting the fascinating intrinsic properties of graphene, is a developing three-dimensional scaffold material [1-2]. GA aerogel shows excellent mechanical strength, ultra-low density, highly interconnected pore structure, large specific surface areas, and high electrical conductivity [3-7]. Meanwhile, the outstanding properties of GA enable it promising for applications, for example, supercapacitors, lithium-ion batteries, sensors, and environmental remediation [8-13]. To prepare GA, such methods and processing techniques as self-assembly [14-17], template method [18-20], 3D printing method [21,22], solution freeze-drying [23] have been explored. Particularly, self-assembly has become a popular approach by offering advantages including mild conditions and tunable reaction parameters [24] and has become the most common strategy to construct GA [15].

Normally, for the self-assembly of GA, hydrothermal treatment (50~200 °C) is taken on GO suspension at atmospheric or autogenous pressure in an autoclave [25]. Under the action of the reducing agent and high temperature, GO precursors assemble into graphene hydrogels by removing part of the hydrophilic groups and reconstructing via π−π stacking interactions [26-28]. To ensure that the GOs are sufficiently reduced and the interactions between the graphene sheets are strong enough, the hydrothermal reduction process usually takes 6 to 24 hours [29-31]. Afterward, the hydrogel is frozen, and the ice

templating effect enables reduced graphene oxide (rGO) sheets to form the solid walls of the cellular structure. The GA is subsequently obtained from this hydrogel by freeze-drying [32]. However, by using this method, the conductivity and elasticity of the attained GA are not always desirable [33]. To enhance its properties, post-treatments like annealing are usually required. As a result, the entire manufacturing process ends up complicated, time-consuming, and costly. Clearly, it remains challenging to fabricate GA via an economic and rapid approach.

There were reports on the use of microwave irradiation to reduce GO within a short time early in 2010 [34-37]. Graphite or pure graphene with abundant delocalized π electrons can convert microwave energy into heat energy efficiently via Joule heating [38]. Therefore, microwave irradiation can lead to a fast temperature increase of GO, facilitating rapid removal of oxygen-containing group on timescales that are too short to undermine graphene sheet stability [39,40]. Simple, quick microwave treatment becomes a desirable method to prepare high-quality reduced graphene, providing us an inspiration for the rapid preparation of GA. However, it was reported that GO is a poor microwave absorbing material, and only the unoxidized graphitic region "impurities" in GO and trace amounts of rGO are the real parts which act as the microwave absorbents to initiate the microwave-induced deoxygenation [41]. During the reduction process, once the number of oxygen groups on the GO decreases and the sp^2 structure is partially restored, the formed rGO with enhanced microwave absorption capacity can generate more heat which subsequently promotes further reduction of GO [42].

In this work, we reported a facile, rapid method for GA fabrication. With the aid of

thiourea, partially reduced graphene hydrogel (PGH) could be formed from GO and thiourea mixture through as short as 30 min of hydrothermal process. After the freeze-drying of PGH, partially reduced GA (PGA) was obtained. Then the PGA was exposed to microwave irradiation, allowing the further reduction of rGO sheets. It is worth noting that the purpose of the hydrothermal reduction is to develop a 3D scaffold with GO and to enable GO sheets more receptive to microwaves, thereby improving the efficiency of the deoxygenation process. By manipulating the microwaving time, MGA-10, that is, GA microwaved for 10 s, exhibits ultra-low density (1.8 mg/cm^3), excellent elasticity, and remarkable compressibility (90%). The oil adsorption capacity and recycling performance of MGA-10 for different oils and organic solvents was investigated. MGA-10 exhibits high adsorption capacity, for example, reaching up to 430 g/g for toluene. The electrical resistance of MGA-10 is highly variable upon strain, allowing MGA-10 to act as a potential pressure sensor with high sensitivity (1.12 kPa^{-1}), good structural stability, and sensing durability (3000 cycles at 70% compression strain).

2. Experimental

2.1 Materials

Graphite powder (≥325 mesh) and phosphorus pentoxide (P_2O_5) were purchased from Aladdin (Shanghai, China). Ammonium persulfate ($(NH_4)_2S_2O_8$), potassium permanganate ($KMnO_4$) and hydrogen peroxide (H_2O_2) were obtained from Tianjin Damao Chemical Reagent Co., Ltd. Sulfuric acid (H_2SO_4) and hydrochloric acid (HCl), were purchased from Tianjin Fengchuan Chemical Reagent Co., Ltd, and thiourea was

purchased from Tianjin Kemiou Chemical Reagent Co., Ltd. was purchased from All chemicals were used without further purification.

2.2 Preparation of GO dispersion

The graphene oxide (GO) dispersion was prepared by an improved Hummers method [43]. The graphite powder (2 g, 325 mesh), $(NH_4)_2S_2O_8$ (2 g) and P_2O_5 (2 g) were put into H_2SO_4 solution (98%, 10 mL) successively, followed by stirring at 80°C for 4h. The mixture was washed with deionized water until the pH value of the filtrate turned to neutral. The filtered solid was dried in a vacuum atmosphere for 2 h to obtain the pre-oxide graphite. 0.6 g of pre-oxide graphite was put into H_2SO_4 solution (98%, 24 mL), in an ice bath and stirring. 3 g of $KMnO_4$ was slowly added under the same circumstance. Then, the mixture was heated to 35°C for 2 h. Subsequently, the temperature was raised to 95°C for 30 min. After cooling to the room temperature, the reaction was terminated by adding deionized water (200 mL) and the H_2O_2 solution (30%, 6 mL). The mixture was washed with HCl solution (volume ratio: HCl: water 1:10) for 4 times, and with deionized water to neutral to remove the residual metal ion. After 2h ultrasonication in a low temperature (<10℃), the graphene oxide dispersion was obtained.

2.3 Preparation of partially reduced graphene aerogel (PGA)

The concentration of the GO solution was adjusted to 2 $mg \cdot mL^{-1}$ and form a dispersion by repeat ultrasonication. Designated amount of reducing agent (thiourea) was added to GO solution. The mixture was heated to 98°C for 30 min to obtain a partially reduced graphene hydrogel (PGH). The resultant hydrogel was immersion in

alcohol-water mixture solution (the volume ratio is 9:1) for 6h. Afterward, PGH was freeze-dried for 36 h to obtain PGA. The obtained MGAs with different hydrothermal reduction times were marked as X-MGA, in which X represents the hydrothermal reduction time.

2.4 Preparation of microwave-treated graphene aerogel (MGA)

PGA was microwave treated with different times (4, 6, 8, 10 and 12 s) in a nitrogen atmosphere to obtain MGA. These graphene aerogels were denoted as MGA-t, where t stands the microwave treatment time.

2.5 Characterizations

Scanning electron microscopy (SEM) was carried out with Shimadzu JSM-6380LV instrument. The transmission electron microscope (TEM) was carried out with field FEI Tecnai F20 emission transmission electron microscope. XRD analysis was conducted on Mini Flex II X–ray diffractometer with diffraction angle range of 5~75°, with a scan rate of 4°~5°/min. The XPS measurements were performed on ESCALAB 250Xi. The contact angle was measured on a JC-2000C Contact Angle Measuring Instrument. The electrical properties of the aerogels were measured using RIGOL DM3068 digital multimeter. The BET tests were performed on BeiShiDe instrument (PM1-1180-A). The dynamic mechanical analysis (DMA) was carried out with GABO Eplexor instrument (6000N).

2.6 Mechanical Testing

The compressive mechanical properties of MGA were tested on a Uniaxial Materials Testing System (LIGAO, HF-9002) equipped with a 10 kg load cell at room

temperature. The compressive tests were conducted using a cylinder-shaped MGA specimen (18 mm in diameter and 14 mm in height) at 100 mm·min^{-1}.

2.7 Adsorption performance evaluation

To investigate the adsorption performance of the graphene aerogels, a weighted amount of MGA was soaked into different organic solvents at room temperature. The aerogel was weighted every two minutes and blotted with the filter paper until the mass remained constant. The absorption capacity (W) of MGA is calculated by Equation (1):

$$W = (M_t - M_0)/M_0 \quad (1)$$

where M_0 (g) and M_t (g) are the mass of the aerogel before and after the absorption, respectively.

2.8 Pressure Sensor Design and Testing

MGA was sandwiched between polyimide layers and connected with the copper wire for assembly of the pressure sensor. The sensor was connected with a computer and the Uniaxial Materials Testing System. Electrical signals of the strain sensor were recorded by RIGOL DM3068 digital multimeter at 1 V.

2.9 Subtle Pressure Monitor Design and Testing

This subtle pressure sensing device is made from the digital multimeter, propulsion device and MGA sensor with a vessel fasten on the top to collect the water droplets. The propulsion device extrudes the water droplets at a constant flow rate (100 mL/h), while the MGA sensor receiving the water droplets and causing electrical signals. The MGA sensor is connected to a digital multimeter for the signal processing and a computer for outputting the signal.

3. Results and discussion

3.1 Fabrication and characterizations of MGA

Fig. 1a illustrates the schematic diagram of preparing MGA by a two-step reduction method, i.e., hydrothermal reduction followed by microwave treatment. In the first hydrothermal reduction process, thiourea was quickly added to GO solution with stirring, and the mixture was then heated to 95 ℃ and remained for 30 min. During this process, the mixture gradually turned to black from brown (Fig. S1) and then self-assembled into partially reduced graphene hydrogel (PGH). Thiourea is a powerful reducing agent, which can partially reduce GO and enable GO to self-assemble into stable hydrogels in a short time. In the control experiment without thiourea, the hydrothermal process could not reduce GO into a regularly shaped hydrogel even after 3h (Fig. S2). With thiourea as the reducing agent here, when the hydrothermal time is less than 30 min, it is too short to form a stable PGH. When the reduction time is longer than 30 min, the obtained MGA becomes denser and the volume decreases (Fig. S3a). After dialyzed in the water-alcohol mixture (the volume ratio of water to alcohol was 9:1), PGH was freeze-dried to form PGA. Then, microwave treatment was adopted on PGA in a nitrogen atmosphere to complete the second reduction to obtain MGA (Fig. S3b). During the microwave treatment process, the temperature of PGA quickly increased and arc can be clearly observed (Fig. S4, Video S1). Meanwhile, with the violent reaction, white smoke was constantly produced. Digital photographs of PGA and MGA are presented in Fig. 1b, demonstrating that the color of PGA turns from black to gray with metallic lustre after the microwave treatment. The color change of PGA is owing to the redshift of light caused by the restoration of π–π conjugation of graphene sheets in MGA [43,44]. The obtained highly restored graphene sheets show a higher reduction level. With increasing the reduction level, a dark black color with no

lustre would gradually turns gray with metallic lustre [41,45]. Since the restoration of π–π conjugation and reduction process took place on every graphene sheet, it is a process without distinction between the internal and external, so not only the surface but also the interior become gray with metallic lustre as shown by Fig. S5. MGA exhibits ultra-low density, being supported by two human hairs (Fig. 1c); meanwhile, MGA shows super compressibility, being able to withstand a weight which is more than 1600 times mass of itself and recover to its original state without any damage (Fig. 1d).

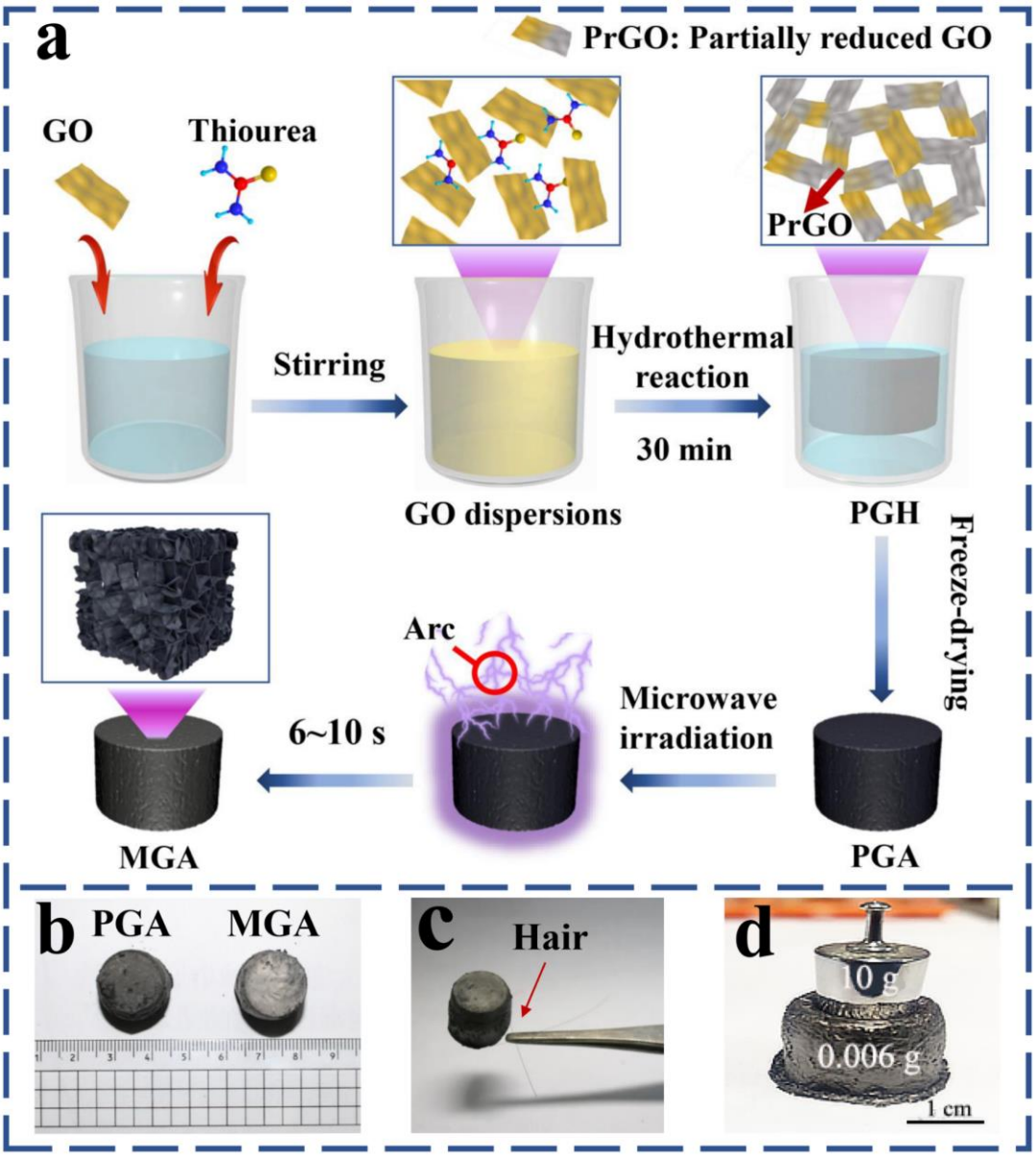

Fig. 1. (a) Schematic diagram of the fabrication process of MGA, (b) digital photographs of PGA and MGA-10. Digital photographs showing MGA-10 (c)

supported by two human hairs and (d) withstanding a weight more than 1600 times mass of itself.

The conversion of GO to MGA was achieved via two-step reduction steps. There are two purposes for the first partially reduction: 1) to facilitate GO sheets to self-assemble into a 3D scaffold with the assistance of thiourea by decreasing the electrostatic repulsion between neighboring GO layers; 2) to promote the second reduction via the partially reduced GO sheets which are much more receptive to microwaves than pristine GO. The reduction mechanism of GO by thiourea and microwave treatment is illustrated in Fig. 2. Thiourea first partially reduces GO sheets by removing oxygen-containing functional groups. The Vander waals force and enhanced π-π interactions between neighboring graphene flakes, along with hydrogen bonding between new functional groups such as amino ($–NH_2$) and sulfonic acid ($–SO_3H$) induced by thiourea [46], drive GO to self-assemble into a robust cellular scaffold during the hydrothermal process in as short as 30 min. These newly formed functional groups enable strong crosslinks between the adjacent GO sheets. Meanwhile, increased the partially reduced to rGO, leading to increased hydrophobicity and therefore enhanced oil-water separation ability [14]. Afterward, the high temperature generated by microwave treatment, allowing most functional groups containing oxygen, nitrogen and sulfur atoms to be eliminated in the form of such gases as ammonia, hydrogen sulfide, and carbon dioxide, which can be confirmed by remarkably reduced N, S elements by converting PGA to MGA (5.09 to 1.54 at. % for N and 4.66 to 1.51 for S) in Table S1. In the meantime, a dramatic weight loss of up to 60% from PGA to MGA was measured (Fig. S6), which is possibly ascribed to the decomposition of thermally labile oxygen functional groups [47].

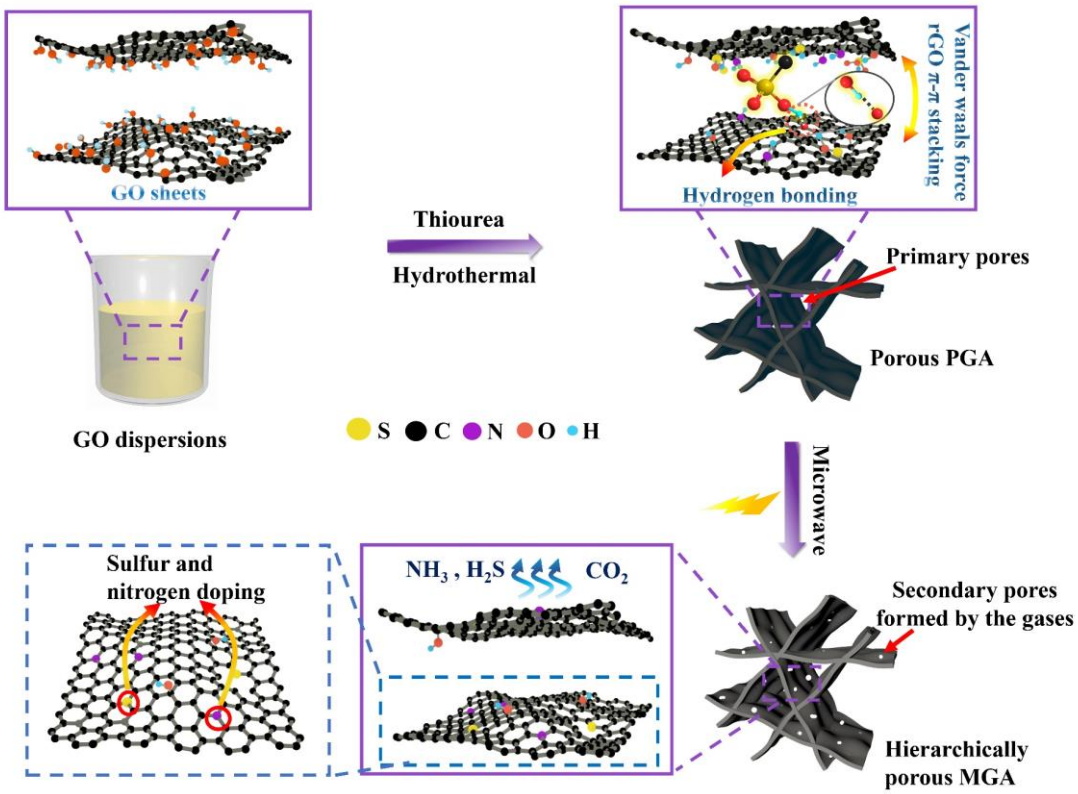

Fig. 2. Schematic illustration of the two-step reduction mechanism of converting GO to MGA.

Fig. 3a, b presents surface and side SEM images of the self-made GO. Each GO consists of continuously aggregated sheets with a wrinkled surface. Significant differences in the morphology and microstructure of PGA and MGA could be observed by SEM images. PGA possesses highly interconnected pores (ranging from ~50 to 100 μm), built by relatively smooth solid walls (Fig. 3c, d). MGA maintains the porous structure and displays a cellular microstructure (Fig. 3e, f). It is worthy to note that newly formed numerous secondary pores (ranging from ~0.7 to 3.8 μm) are observed on the cell walls of MGA (as indicated in Fig. 3f). It is proposed that the burst of volatilized gases, engendered by the high temperature ascribed to the absorption of microwave by the reduced graphene sheets, break through the walls and therefore give rise to new micropores in addition to existing primary pores. This hierarchically porous structure imparts MGA with excellent compressive-resilient and lightweight

characteristics, rendering it promising candidates for applications such as oil adsorption and sensing. TEM images reveal the wrinkled and folded surface of graphene sheet of MGA (Fig. 3g). The thin graphene nanostructures consist of 2-5 layers from HRTEM images in Fig. 3h. The high temperature during microwave treatment leads to partially graphitization of PGA, which takes in the form of graphite strip, [48] the d-spacing value of which is 0.376 nm (Fig. 3i).

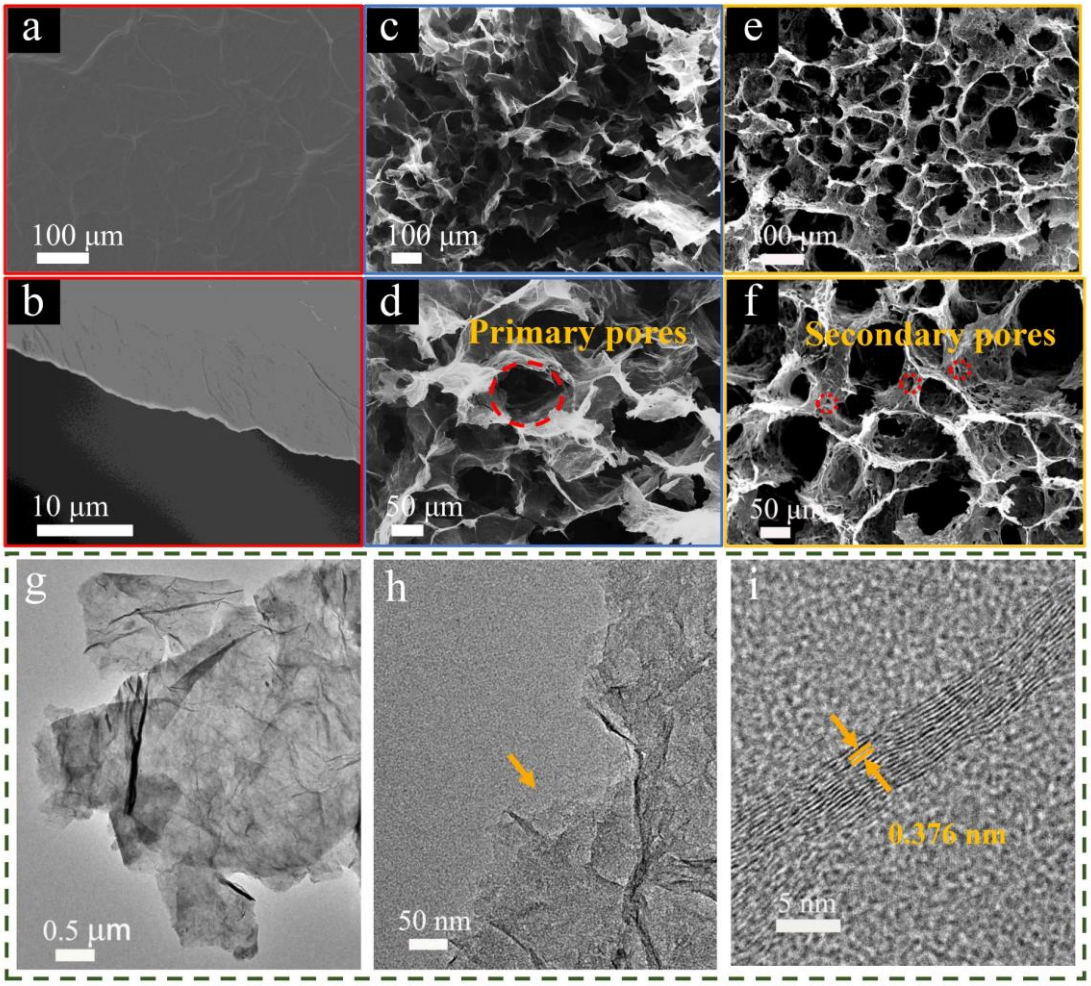

Fig. 3. Morphology and microstructure. SEM images of (a-b) GO, (c-d) GA and (e-f) MGA at different magnifications. (g) TEM and (h-i) HRTEM images of MGA.

The crystalline structures of GO, PGA and MGA are demonstrated by XRD patterns in Fig. 4a. The sharp (001) diffraction peak of GO (2θ=11.7°) completely disappears for both PGA and MGA. The diffraction (002) peaks for the graphitic carbon structure shifts from 21.6° for PGA to 25.7° for MGA, indicating the second reduction of PGA

during the microwave treatment [49]. The d-spacing of MGA is 3.5 Å, much lower than that of GO (7.26 Å) and slightly lower than that of PGA (3.72 Å). The removal of surface functional groups from graphene sheets contributes largely to the improved interconnectivity. The decreased d-spacing also suggests restoration of the graphitic structure. The microwave treatment diminishes the interlayer distance of the graphene sheets. Besides, XRD patterns of control groups with different microwave treatment times (4, 6, 8, 12 s, hydrothermal reduction time: 30 min) and different hydrothermal reduction times (30, 45, 60 min, microwave treatment time: 10 s) are presented in Fig. S7 and S8, respectively. As the microwave treatment time increases, the 002 diffraction peaks of MGA is getting shaper, indicating higher reduction degree and reduced structural defects [50]. When the microwave treatment exceeds 10 s, the change of the 002 peak is not obvious, suggesting that 10 s is longer enough to reduce MGA. Interestingly, the MGAs with different hydrothermal reduction times exhibit almost overlapping XRD curves (Fig. S8). It can be deduced that different hydrothermal times may lead to varying reduction degree of PGA, but these PGAs were sufficiently reduced to a close reduction degree by the high temperature occurred in the subsequent 10 s of microwaving process.

Fig. 4b shows the Raman spectra of GO, PGA and MGA. The two characteristic peaks at 1335 cm^{-2} and 1585 cm^{-2} assigned to D and G-bands of carbon, reflect disordered sp^3 and ordered sp^2 carbon domains, respectively [50, 51]. The relative peak intensity ratio of the D to the G band (I_D/I_G), revealed the defects and disorder in the carbon structure [52]. It is notable that I_D/I_G decreases from 1.23 for GO to 1.12 for PGA, and 0.95 for MGA, suggesting the removal of defects in PGA and increased graphitization in MGA.

Four main elements of carbon, nitrogen, oxygen, and sulfur exist from XPS survey

spectra (Fig. 4c). There are a N1s peak (400.1 eV) and a S2p (165.0 eV) peak in the spectra of PGA, which are possibly introduced by thiourea [53]. Interestingly, the intensity of these two peaks decreased remarkably after the microwave treatment, which is caused by the exhausting of N and S elements in the form of oxide gases. The atomic contents of N and S elements are 5.09 and 4.66 at.%, respectively, in PGA, and decrease to 1.54 and 1.51 at.%, respectively, in MGA (Table S1). Moreover, the peak intensity corresponding to O1s (532.8 eV) decreases while that of C1s (285.7 eV) increases. The C/O atom ratio is 1.67 for GO, and is increased to 3.9 for PGA, and to 42.7 for MGA, indicating the elimination of oxygen-containing groups of PGA and MGA during the two-step reduction process. Fig. 4d shows the high-resolution spectrum of the C1s region of GO, PGA and MGA. GO exhibits three individual peaks at 284.85, 287.05, and 288.8 eV attributed to C-C, C-O, C=O, respectively (Fig. 4d i) [54]. By comparing GO with PGA, two extra peaks at 286.0 eV and 285.3 eV are responsible for C-N and C=S bond, respectively, (Fig. 4d ii)[32,55] introduced by thiourea. With the further reduction by microwave treatment, the intensity of these two bonds were notably decreased, providing strong evidence for the discharge of N, S element containing gases. Nevertheless, these two peaks remained in Fig. 4d iii, indicating the doping of S and N elements of MGA. The existence of N, S elements in MGA can be seen much more clearly in the SEM elemental mapping (Fig. S9).

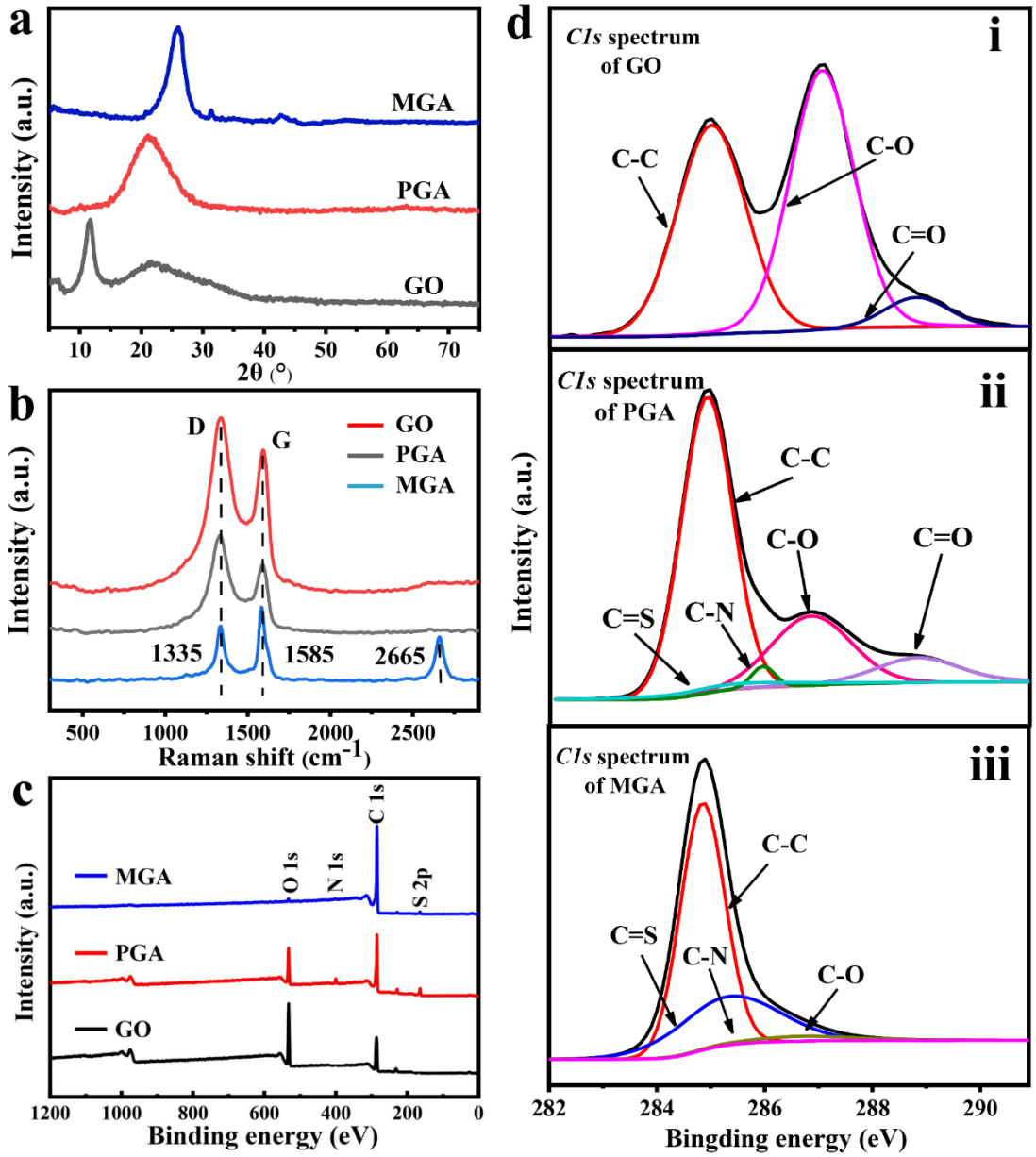

Fig. 4. Crystalline and chemical structure. (a) XRD patterns, (b) Raman spectra, (c) XPS spectra, and (d) high resolution of C1s spectra of GO, PGA and MGA-10.

3.2 Mechanical properties

The obtained MGA is capable of recovering to its original shape after being compressed to a large compressive strain by a weight of 50 g, as shown in Fig. 5a and Video S2, suggesting an excellent compressive elasticity. Even after extremely strains reaching up to 90%, MGA can still return to its original shape without collapse (Video S3). The compressive stress-strain curves of MGA with different microwave treatment times (6, 8, 10, and 12 s) and compression strains (50%, 80%, and 90%) are

demonstrated in Fig. S10 and Fig. 5b. Similar to other graphene aerogels, the compressive stress-strain curves of MGA show linear elasticity, plateau, and densification regimes during the compression process. With increasing the microwave treatment time, the maximum compressive stress at a constant strain demonstrates a significant decrease (Fig. 5c). It is due to the newly formed secondary pores on cell walls in MGA, allowing the MGA much easier to deform. Compared with PGA, MGA processes both better compressibility and superelasticity. The compressive strength at 90% strain for MGA-10 was only 10.07 kPa. This remarkable compressibility allows any oil or organic solution adsorbed by MGA-10 to be removed effortlessly. In addition, the durability of MGA-10 is demonstrated by the repeated loading-unloading 100 cycles at a strain of 80% (Fig. 5d). The ultimate stress decreased only 10.3% after 100 cycles. The loading-unloading curves almost overlapped each other with increasing the cycle number, indicating an outstanding structural stability and repeatability. To better reveal the effects of microwave treatment, the height recovery ratio of MGA-10 and PGA was investigated (Fig. 5e). MGA could maintain 91.5% recovery ratio after 10 compression cycles (@90% compressive strain). However, PGA was permanently deformed after only 1 cycle of compression (Fig. S11). It can be revealing that a 30 min hydrothermal process is insufficient for graphene sheets to remove the oxygen-containing functional groups (Fig. 4c by the XPS analysis and atomic composition in Table S1). The interactions between these functional groups makes PGA rigid and inelastic. The secondary pores formed by the microwave treatment also contributes to improved resilience of MGA.

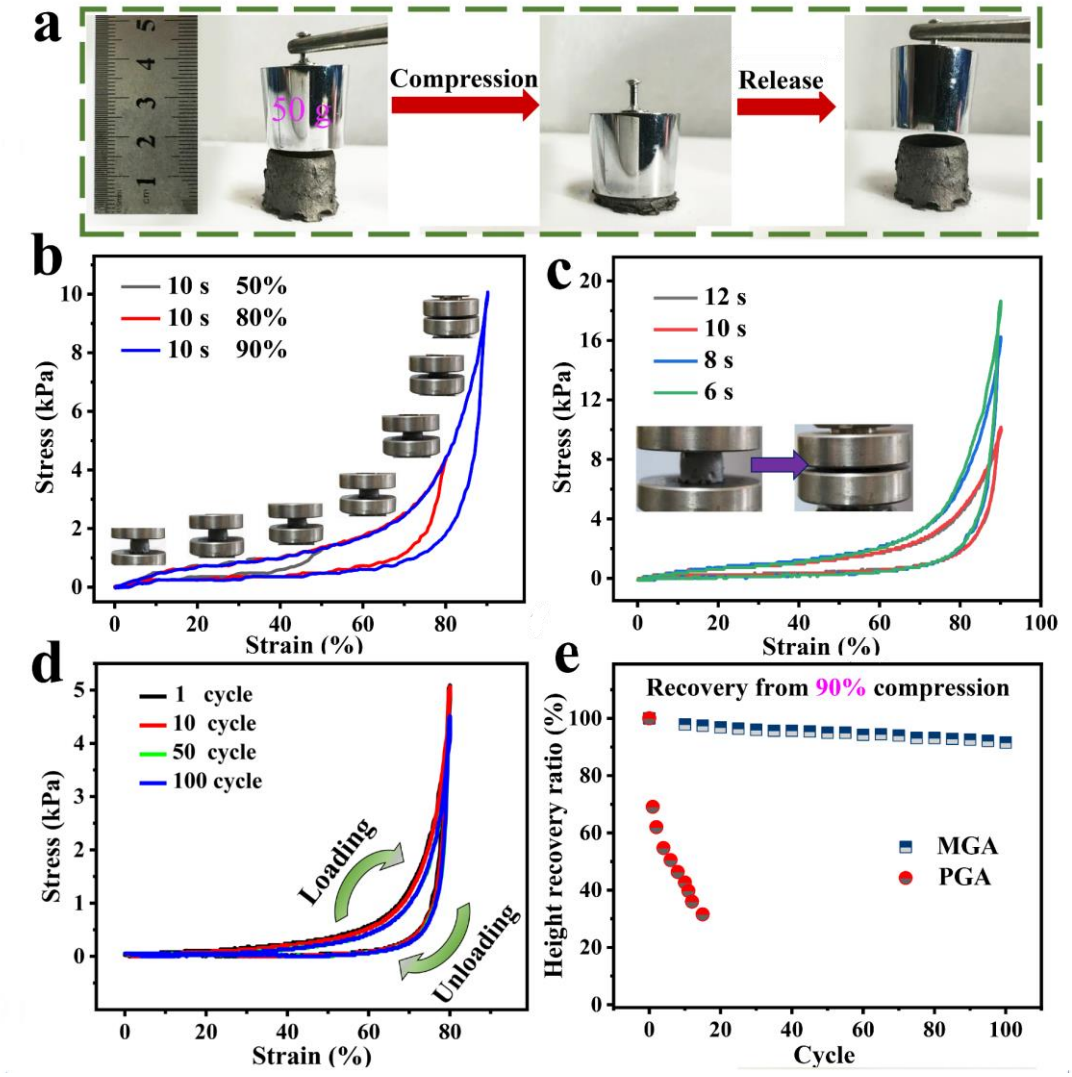

Fig. 5. Mechanical properties of PGA and MGA-10. (a) Digital photographs showing compression and recovery process of MGA-10. (b) Compressive stress-strain curves of MGA-10 under different compression strain. (c) Compressive stress-strain curves of MGA with different microwave treatment time. (d) Cyclical performance of MGA-10 when compressed at 80% and released for 100 cycles. (e) Height recovery ratio of MGA-10 and PGA from 90% compression for 100 cycles.

3.3 MGA for oil-water separation

MGA, with an ultralow density and hierarchically porous structure, is expected to be promising for oil adsorption. MGA-10 possesses hydrophobic (with a contact angle of 132°, Video S4) and oleophilic properties (Fig. 6a, Video S5) and can absorb the oil on the surface and under water quickly (Fig. 6b, Video S6-7). Comparing with PGA, MGA-10 exhibits larger absorption capacities toward a wide range of oils and organic solvents, including peanut oil, gasoline, diesel oil, pump oil, n-heptane, chloroform,

and toluene (Fig. 6c). Particularly, the adsorption capacity of MGA toward toluene reaches as high as 430 $g \cdot g^{-1}$. This is due to the lower density and much more pore structures of MGA-10. These newly form secondary pore structures generating in the microwave treatment provide MGA-10 a larger specific surface area (177.7 m^2/g) than PGA (141.2 m^2/g) from Fig. S12. Comparing with groups obtained by different hydrothermal reduction time (30-MGA, 45-MGA, 60-MGA), the 30-MGA possesses larger internal space for adsorbing oil. For 45-MGA and 60-MGA, the internal space is smaller than that of 30-MGA. As a result, there is not enough space to store the absorbed oil or solvents (Fig. S13) In the comparison between MGA-10 and other microwave treatment time groups (MGA-4, MGA-6, MGA-8, MGA-12), MGA-10 still shows excellent performance in oil absorption (Fig. S14). The MGAs at shorter microwaving time (4, 6, 8 s) were not sufficiently reduced by microwave treatment, and thus have fewer secondary pore structures and greater self-weight. MGA-10 almost retains its original adsorption performance after 10 adsorption/burning cycles (Fig. 6d, and the adsorption/burning process is presented in Fig. S15) and maintains 83.5% of the original absorption capacity after 10 adsorption/squeezing cycles (Fig. 6e). For other oils, for example, pump oil, MGA-10 also kept 71.2% of the original absorption capacity after 10 adsorption/burning cycles (Fig. 6f). These results suggest that MGA-10 is a promising candidate for oil-water separation.

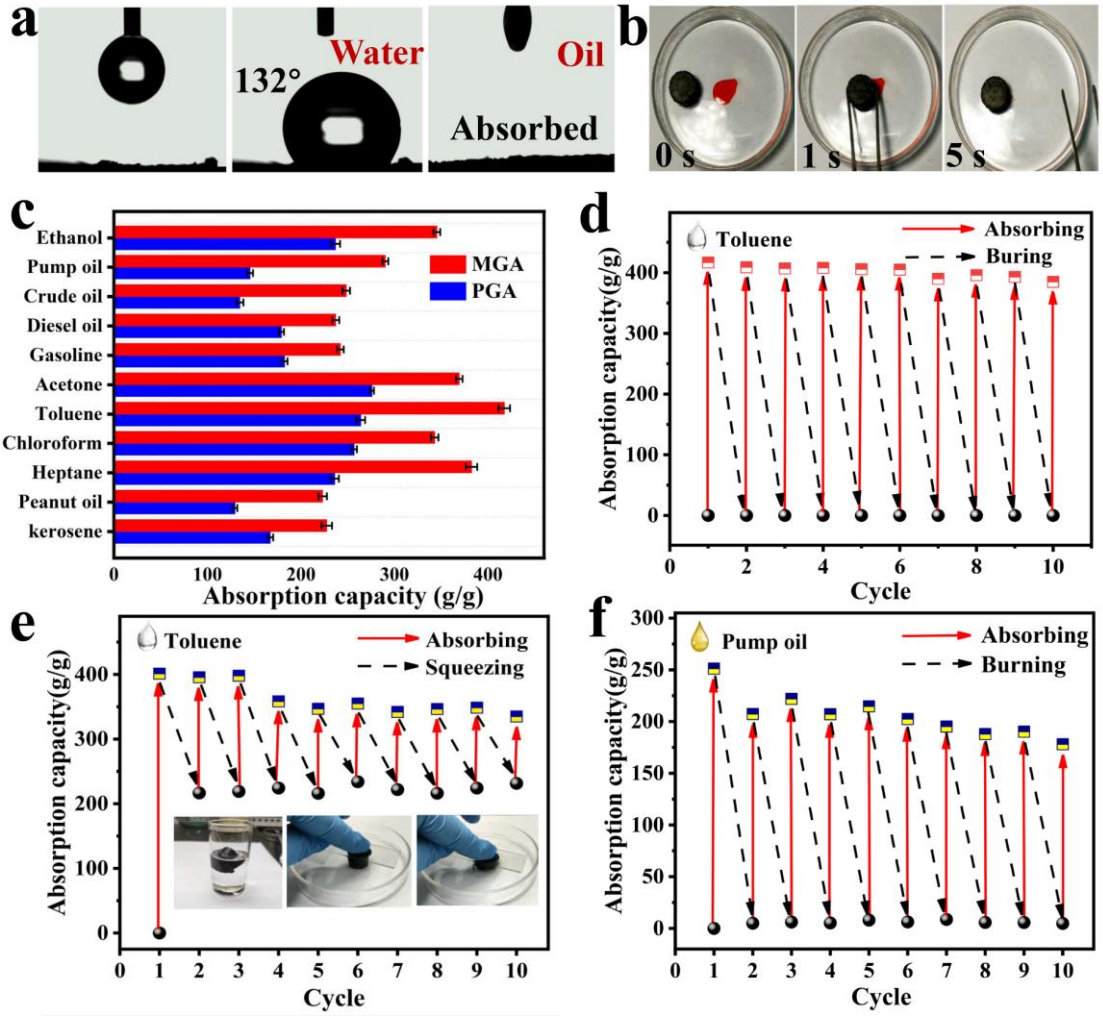

Fig. 6. (a) Superhydrophobic MGA with a water contact angel of 132° and exhibits fast permeation of oil into MGA-10. (b) Digital photographs showing absorption of toluene (stained with Sudan III) on water by MGA-10. (c) Comparison between the absorption capacities of PGA and MGA for various oils and organic solvents. (d-e) Absorption-burning cycles and absorption-squeezing (50%) cycles of MGA-10 for toluene. (f) Absorption-burning cycles of MGA-10 for pump oil.

3.4 Electromechanical properties of MGA

The highly repeatable compressibility and high sensitivity of electrical conductivity to the compressive strain (Fig. S16) enables MGA-10 a suitable candidate for pressure sensors. The cellular walls of MGA are closely compressed together during compression, leading to more compact stacking and reduced electrical resistance. The pressure sensing performance of the MGA-10 pressure sensor was evaluated by an experimental setup including a digital multimeter, a mechanical motion controller, and a computer (Fig. S17). Fig. 7a shows the relative resistance-change pressure curve of

the MGA-10 sensor. The pressure sensitivity S is defined as $S = \delta(\Delta R/R_0)/\delta P$ with $\Delta R = (R - R_0)$, where R and R_0 represent the resistance of the sensor with and without the pressure, respectively, and P is the applied pressure. The curves are divided into three parts. From the slope of linear fitting curves, S_1 is 1.112 kPa^{-1} in the pressure range of 0~0.3 kPa, S_2 is 0.0832 kPa^{-1} in the pressure range of 0.328~4.11 kPa, and S_3 is 0.032 kPa^{-1} in the pressure range of 4.23~18 kPa, respectively. Due to their much denser internal structure, 45-MGA and 60-MGA require greater stress to generate the same deformation as 30-MGA. As a result, the sensitivity of 45-MGA and 60-MGA is not as higher as that of 30-MGA (Fig. S18). In the comparison between MGA-10 and other microwave treatment time groups, MGA-10 exhibits higher sensitivity (Fig. S19). It can be deduced that the samples not sufficiently reduced (MGA-4, MGA-6, MGA-8) have more remained oxygen-containing groups on their graphene sheets and less secondary pores on their graphene walls, which makes them require greater stress to reach the same $\Delta R/R_0$ as the MGA-10. MGA-10 and MGA-12 demonstrate similar oil-water separation and piezoresistive sensing performances, further proving that 10 s is longer enough to well reduce MGA. As illustrated in Fig. 7b, the $\Delta R/R_0$ variations at different strains are quite stable and repeatable. MGA-10 exhibits significant sensitivity changes of the $\Delta R/R_0$ upon pressed and quickly returns to the initial state when the external stress was removed (Fig. 7c). Fig. 7d and 7e show the compressive strain-sensing behavior of the MGA-10 sensor at low frequencies (0.03~0.15 Hz) and high frequencies (0.25~1 Hz), respectively. MGA-10 sensor can detect and respond stably with different frequencies. DMA test has been completed and the result is shown by Fig. S20. It can be seen that at low frequencies, the MGA possesses a greater storage modulus and smaller loss modulus and tanδ. This is because when the frequency is low, the graphene aerogel has enough time to recover. As the frequency increases, the

aerogel exhibits reduced storage modulus and increased loss modulus and tanδ, which is ascribed to the rich porous structure of MGA that needs longer time to recover. Nevertheless, the MGA still responds quickly enough to give frequency-independent $\Delta R/R_0$ signals as proved by Fig. 7e. Fig. 7f demonstrates that after 3000 cycles at 70% compression strain, negligible fluctuations were observed for the sensitivity changes of $\Delta R/R_0$, indicating the excellent structural stability of MGA-10. Loaded with a fast step strain of 5%, the response and recovery times of MGA-10 sensor were measured to be 135 ms and 130 ms, respectively, revealing a fast signal response (Fig. S21).

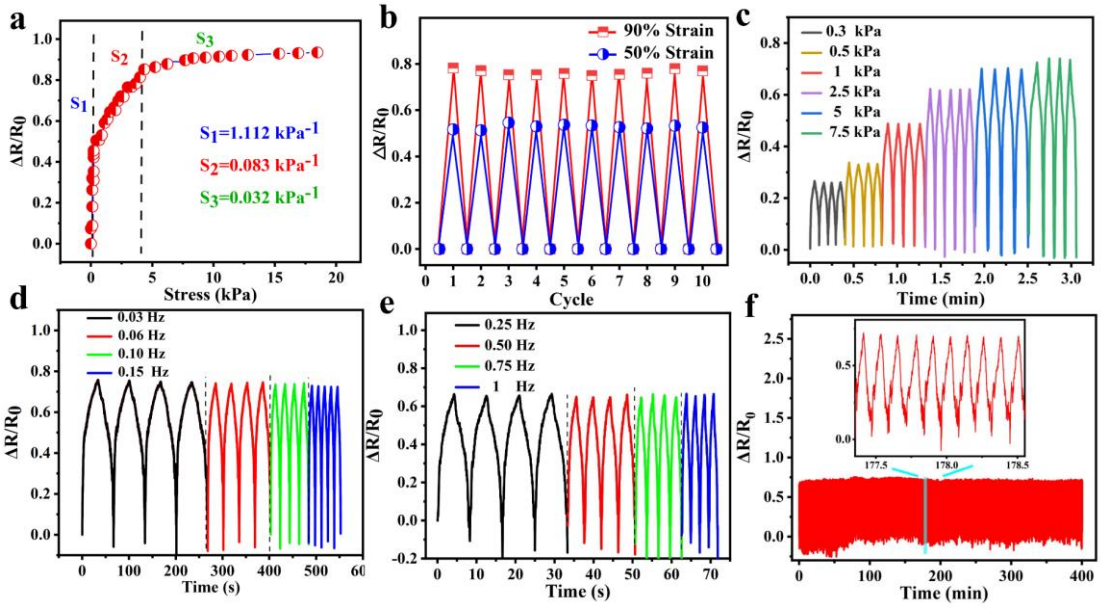

Fig. 7. (a) Relative resistance changes with respect to applied pressures. (b) Cyclic variations of $\Delta R/R_0$ at two compressive strains of 50% and 90%. (c) $\Delta R/R_0$-time curves of MGA-10 under different pressures. (d) $\Delta R/R_0$ changes at low (0.03~0.15 Hz) and (e) high (0.25~1 Hz) frequencies under 50% strain. (f) $\Delta R/R_0$-time curves of MGA-10 under repeated loading-unloading tests with 3000 cycles at 70% compression strain.

Table 1 compares the sensitivity and linear range of MGA-10 with other reported studies. MGA-10 exhibits a much higher sensitivity and moderate linear range.

Table 1. A comparison of the pressing performance between MGA-10 with other graphene-based sensors

Materials	Sensitivity (kPa^{-1})	Pressure regions	Ref.
Graphene and porous	0.33	0~1.5 kPa	[56]

nylon networks			
rGO foam/FPCB	0.13	0~10 kPa	[57]
Graphene/CNT	0.15	0~6 kPa	[58]
Graphene/borophene nanosheets	0.9	0~3 kPa	[59]
Graphene/MXene-PDMS @ sponge	0.053	0~15 kPa	[60]
PPy/rGO@carbonized PU	0.635	—	[61]
Cu NWs/rGO/MF	0.011	0~1.5 kPa	[62]
Graphene/PU sponge	0.26	0~3 KPa	[63]
MGA	1.112	0~ 0.3 kPa	This work

3.5 Demonstration for Real-Time Pressure Monitoring

As a proof of concept, a sensing device was designed from MGA for the real-time pressure monitoring, for example, the subtle pressure hit on a substrate by the water droplet (Fig. 8a). This sensing device is composed of multimeter, propulsion device and MGA sensor with a copper vessel to collect the water droplets. The vertical distance between the tip of the syringe and the bottom of the copper container is 7.8 cm. As the propeller pushes forward, a water droplet gradually forms at the tip of the syringe and falls down. When the water droplets hit and remains at the top of the sensing device, the $\Delta R/R_0$ signals are collected and processed to output the corresponding pressure. In Fig. 8b, the signals generated by water droplets are collected at a flow rate of 100 mL/h. Since the obtained pressure is within 0~0.3 kPa, the sensitivity is S_1 (1.112 kPa^{-1}), and the pressure value is calculated according to Equation (2):

$$\Delta R/R_0 = S_1 \cdot P \quad (2)$$

where $\Delta R/R_0$ is the change in relative resistance caused by the water droplet, S_1 is sensitivity of MGA senor in the pressure range of 0~0.3 kPa, and P is the pressure caused by the falling water droplet. The rang of pressure value is calculated to be 30.2 ±5.5 Pa.

A simulation of falling process of a water droplet (Fig. 8c, Video S8) using the soft

Ansys Fluent 17.2 to verify the reliability of MGA sensor. The simulated pressure generated by the water drop on the MGA sensor is compared with the calculated value by the MGA sensor. The variation of the surface average pressure caused by water droplets with time in the simulation is shown in Fig. 8d, which indicates that the calculated facet average value range of the simulated bottom pressure is 26.4±3.3 Pa. The tolerance between the theoretical value and the simulated value is less than 35.3%. Considering the dissipation of impact force in the transmission process, MGA sensor is reliable for subtle pressure detection.

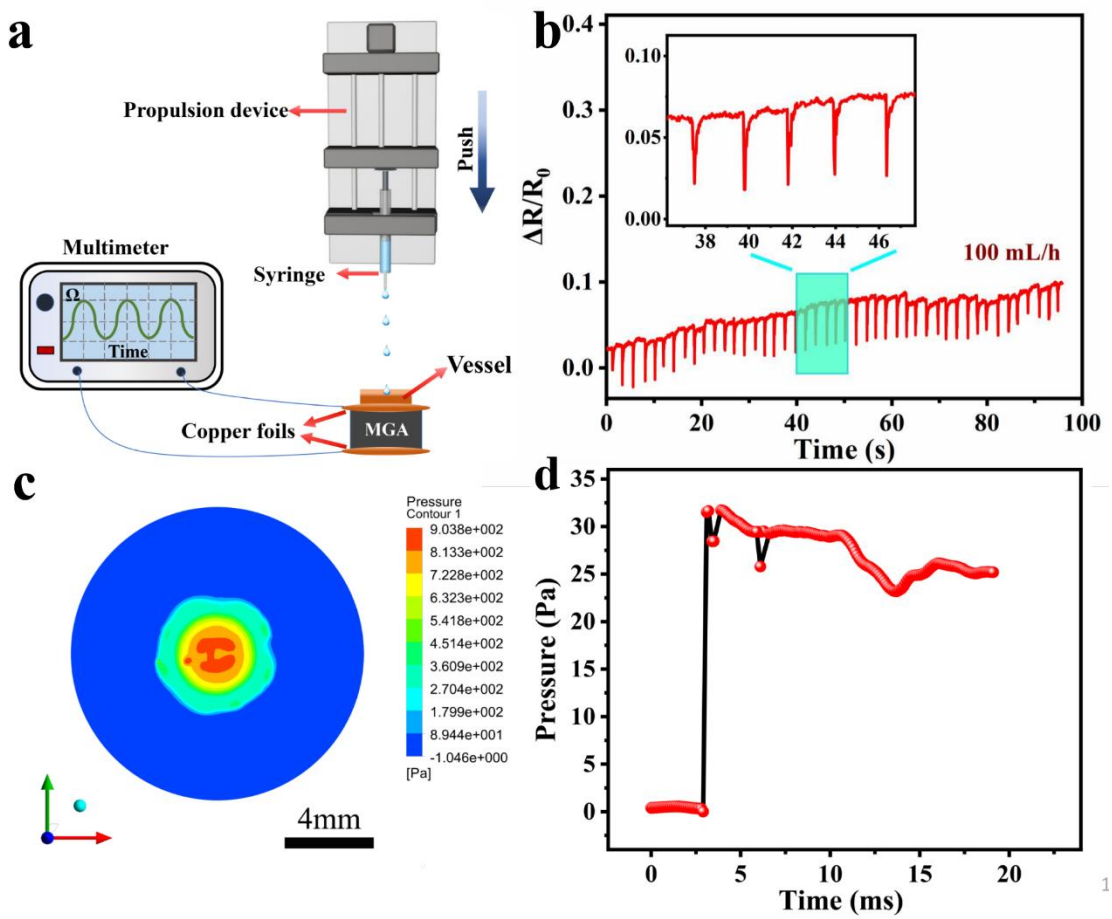

Fig. 8. (a) Schematic of MGA sensing for the real-time pressure monitoring of the water droplet. (b) $\Delta R/R_0$ variations of MGA response to water droplets at a flow rate of 100 $mL \cdot h^{-1}$ (the inset shows $\Delta R/R_0$ signals within 5 seconds). (c) Simulated pressure contour and (d) facet average pressure with time on the upper surface of the MGA sensor.

4. Conclusions

We have successfully fabricated ultralight, hierarchically porous, and high hydrophobic graphene aerogel through a facile self-assembling combined with microwave treatment route. The resultant MGA-10 exhibits a low density of 1.8 $mg \cdot cm^{-3}$, with a resilient strain of 90%. With these merits, the MGA-10 exhibits ahigh adsorption capacities toward various organic solvents and oils. It also shows good reusability. Due to the excellent conductivity and superelasticity of MGA, the pressure sensor based on MGA-10 demonstrates a high sensitivity (1.112 kPa^{-1}) at a pressure range of 0~0.3 kPa and high stability (>3000 cycles). MGA sensor is reliable for subtle pressure monitoring, demonstrating its great potential in the real-time detection of pressures.

Acknowledgement

This work is financially supported by Young Elite Scientists Sponsorship Program by Tianjin (TJSQNTJ-2018-03). The authors would like to thank the Deanship of Scientific Research at Umm Al-Qura University for supporting this work by Grant Code: (22UQU4320141DSR20).

References

[1] C. Zhu, T.Y. Han, E.B. Duoss, A.M. Golobic, J.D. Kuntz, C.M. Spadaccini, M.A. Worsley, Highly compressible 3D periodic graphene aerogel microlattices, Nat Commun, 6 (2015) 6962.

[2] S. Nardecchia, D. Carriazo, M.L. Ferrer, M.C. Gutierrez, F. del Monte, Three dimensional macroporous architectures and aerogels built of carbon nanotubes and/or graphene: synthesis and applications, Chem Soc Rev, 42 (2013) 794-830.

[3] M. Pan, C. Shan, X. Zhang, Y. Zhang, C. Zhu, G. Gao, B. Pan, Environmentally Friendly in Situ Regeneration of Graphene Aerogel as a Model Conductive Adsorbent, Environ Sci Technol, 52 (2018) 739-746.

[4] S. Mahpishanian, H. Sereshti, Three-dimensional graphene aerogel-supported iron oxide nanoparticles as an efficient adsorbent for magnetic solid phase extraction of organophosphorus pesticide residues in fruit juices followed by gas chromatographic determination, J Chromatogr A, 1443 (2016) 43-53.

[5] W. Chen, S. Li, C. Chen, L. Yan, Self-assembly and embedding of nanoparticles by in situ reduced graphene for preparation of a 3D graphene/nanoparticle aerogel, Adv Mater, 23 (2011)

5679-5683.
[6] Z. Qin, G.S. Jung, M.J. Kang, M.J. Buehler, The mechanics and design of a lightweight three-dimensional graphene assembly, Sci Adv, 3 (2017) e1601536.
[7] M.A. Worsley, P.J. Pauzauskie, T.Y. Olson, J. Biener, J.H. Satcher, Jr., T.F. Baumann, Synthesis of graphene aerogel with high electrical conductivity, J Am Chem Soc, 132 (2010) 14067-14069.
[8] Z.S. Wu, A. Winter, L. Chen, Y. Sun, A. Turchanin, X. Feng, K. Mullen, Three-dimensional nitrogen and boron co-doped graphene for high-performance all-solid-state supercapacitors, Adv Mater, 24 (2012) 5130-5135.
[9] R. Wang, C. Xu, J. Sun, L. Gao, Three-dimensional Fe2O3 nanocubes/nitrogen-doped graphene aerogels: nucleation mechanism and lithium storage properties, Sci Rep, 4 (2014) 7171.
[10] T. Alizadeh, F. Ahmadian, Thiourea-treated graphene aerogel as a highly selective gas sensor for sensing of trace level of ammonia, Analytica Chimica Acta, 897 (2015) 87-95.
[11] Z. Xu, Y. Zhang, P. Li, C. Gao, Strong, conductive, lightweight, neat graphene aerogel fibers with aligned pores, ACS Nano, 6 (2012) 7103-7113.
[12] C. Wang, S. Yang, Q. Ma, X. Jia, P.-C. Ma, Preparation of carbon nanotubes/graphene hybrid aerogel and its application for the adsorption of organic compounds, Carbon, 118 (2017) 765-771.
[13] Z. Wang, R. Wei, J. Gu, H. Liu, C. Liu, C. Luo, J. Kong, Q. Shao, N. Wang, Z. Guo, X. Liu, Ultralight, highly compressible and fire-retardant graphene aerogel with self-adjustable electromagnetic wave absorption, Carbon, 139 (2018) 1126-1135.
[14] Y. Xu, K. Sheng, C. Li, G. Shi, Self-assembled graphene hydrogel via a one-step hydrothermal process, ACS Nano, 4 (2010) 4324-4330.
[15] Z.S. Wu, S. Yang, Y. Sun, K. Parvez, X. Feng, K. Mullen, 3D nitrogen-doped graphene aerogel-supported Fe3O4 nanoparticles as efficient electrocatalysts for the oxygen reduction reaction, J Am Chem Soc, 134 (2012) 9082-9085.
[16] X. Zhao, W. Yao, W. Gao, H. Chen, C. Gao, Wet-Spun Superelastic Graphene Aerogel Millispheres with Group Effect, Adv Mater, 29 (2017).
[17] J. Yang, X. Li, S. Han, Y. Zhang, P. Min, N. Koratkar, Z.-Z. Yu, Air-dried, high-density graphene hybrid aerogels for phase change composites with exceptional thermal conductivity and shape stability, Journal of Materials Chemistry A, 4 (2016) 18067-18074.
[18] R. Zhang, Y. Cao, P. Li, X. Zang, P. Sun, K. Wang, M. Zhong, J. Wei, D. Wu, F. Kang, H. Zhu, Three-dimensional porous graphene sponges assembled with the combination of surfactant and freeze-drying, Nano Research, 7 (2014) 1477-1487.
[19] S. Barg, F.M. Perez, N. Ni, P. do Vale Pereira, R.C. Maher, E. Garcia-Tunon, S. Eslava, S. Agnoli, C. Mattevi, E. Saiz, Mesoscale assembly of chemically modified graphene into complex cellular networks, Nat Commun, 5 (2014) 4328.
[20] L. Zhou, S. Zhai, Y. Chen, Z. Xu, Anisotropic Cellulose Nanofibers/Polyvinyl Alcohol/Graphene Aerogels Fabricated by Directional Freeze-drying as Effective Oil Adsorbents, Polymers (Basel), 11 (2019).
[21] Q. Zhang, F. Zhang, S.P. Medarametla, H. Li, C. Zhou, D. Lin, 3D Printing of Graphene Aerogels, Small, 12 (2016) 1702-1708.
[22] Y. Jiang, Z. Xu, T. Huang, Y. Liu, F. Guo, J. Xi, W. Gao, C. Gao, Direct 3D Printing of Ultralight Graphene Oxide Aerogel Microlattices, Advanced Functional Materials, 28 (2018).
[23] H. Sun, Z. Xu, C. Gao, Multifunctional, ultra-flyweight, synergistically assembled carbon

aerogels, Adv Mater, 25 (2013) 2554-2560.
[24] W. Wan, F. Zhang, S. Yu, R. Zhang, Y. Zhou, Hydrothermal formation of graphene aerogel for oil sorption: the role of reducing agent, reaction time and temperature, New Journal of Chemistry, 40 (2016) 3040-3046.
[25] E. Garcia-Bordeje, A.M. Benito, W.K. Maser, Graphene aerogels via hydrothermal gelation of graphene oxide colloids: Fine-tuning of its porous and chemical properties and catalytic applications, Adv Colloid Interface Sci, 292 (2021) 102420.
[26] H. Hu, Z. Zhao, W. Wan, Y. Gogotsi, J. Qiu, Ultralight and highly compressible graphene aerogels, Adv Mater, 25 (2013) 2219-2223.
[27] S. Wu, R.B. Ladani, J. Zhang, K. Ghorbani, X. Zhang, A.P. Mouritz, A.J. Kinloch, C.H. Wang, Strain Sensors with Adjustable Sensitivity by Tailoring the Microstructure of Graphene Aerogel/PDMS Nanocomposites, ACS Appl Mater Interfaces, 8 (2016) 24853-24861.
[28] L. Liang, Q. Li, X. Yan, Y. Feng, Y. Wang, H.B. Zhang, X. Zhou, C. Liu, C. Shen, X. Xie, Multifunctional Magnetic Ti3C2Tx MXene/Graphene Aerogel with Superior Electromagnetic Wave Absorption Performance, ACS Nano, 15 (2021) 6622-6632.
[29] W. Kang, Y. Cui, L. Qin, Y. Yang, Z. Zhao, X. Wang, X. Liu, A novel robust adsorbent for efficient oil/water separation: Magnetic carbon nanospheres/graphene composite aerogel, J Hazard Mater, 392 (2020) 122499.
[30] A.a. Zhou, Q. Yang, K. Xu, Q. Zhou, J. Wu, H. Bai, Manipulating the elasticity of chemically modified graphene aerogel through water surface plasticization, Carbon, 184 (2021) 43-52.
[31] Y. Wang, X. Gao, Y. Fu, X. Wu, Q. Wang, W. Zhang, C. Luo, Enhanced microwave absorption performances of polyaniline/graphene aerogel by covalent bonding, Composites Part B: Engineering, 169 (2019) 221-228.
[32] N. Wei, Q. Wang, Y. Ma, L. Ruan, W. Zeng, D. Liang, C. Xu, L. Huang, J. Zhao, Superelastic active graphene aerogels dried in natural environment for sensitive supercapacitor-type stress sensor, Electrochimica Acta, 283 (2018) 1390-1400.
[33] X. Chen, D. Lai, B. Yuan, M.-L. Fu, Tuning oxygen clusters on graphene oxide to synthesize graphene aerogels with crumpled nanosheets for effective removal of organic pollutants, Carbon, 143 (2019) 897-907.
[34] Y. Guo, B. Chang, T. Wen, C. Zhao, H. Yin, Y. Zhou, Y. Wang, B. Yang, S. Zhang, One-pot synthesis of graphene/zinc oxide by microwave irradiation with enhanced supercapacitor performance, RSC Advances, 6 (2016) 19394-19403.
[35] H.J. Han, Y.N. Chen, Z.J. Wang, Effect of microwave irradiation on reduction of graphene oxide films, RSC Advances, 5 (2015) 92940-92946.
[36] R.R. Mishra, A.K. Sharma, Microwave–material interaction phenomena: Heating mechanisms, challenges and opportunities in material processing, Composites Part A: Applied Science and Manufacturing, 81 (2016) 78-97.
[37] S. Chandrasekaran, S. Ramanathan, T. Basak, Microwave material processing-a review, AIChE Journal, 58 (2012) 330-363.
[38] R. Jakhar, J.E. Yap, R. Joshi, Microwave reduction of graphene oxide, Carbon, 170 (2020) 277-293.
[39] D. Voiry, J. Yang, J. Kupferberg, R. Fullon, C. Lee, H.Y. Jeong, H.S. Shin, M. Chhowalla, High-quality graphene via microwave reduction of solution-exfoliated graphene oxide, Science, 353 (2016) 1413-1416.

[40] V.V. Chaban, O.V. Prezhdo, Microwave reduction of graphene oxide rationalized by reactive molecular dynamics, Nanoscale, 9 (2017) 4024-4033.
[41] S. Tang, S. Jin, R. Zhang, Y. Liu, J. Wang, Z. Hu, W. Lu, S. Yang, W. Qiao, L. Ling, M. Jin, Effective reduction of graphene oxide via a hybrid microwave heating method by using mildly reduced graphene oxide as a susceptor, Appl Surf Sci, 473 (2019) 222-229.
[42] Z. Li, Y. Yao, Z. Lin, K.-S. Moon, W. Lin, C. Wong, Ultrafast, dry microwave synthesis of graphene sheets, Journal of Materials Chemistry, 20 (2010).
[43] H. Hu, Z. Zhao, Q. Zhou, Y. Gogotsi, J. Qiu, The role of microwave absorption on formation of graphene from graphite oxide, Carbon, 50 (2012) 3267-3273.
[44] S. Pei, J. Zhao, J. Du, W. Ren, H.-M. Cheng, Direct reduction of graphene oxide films into highly conductive and flexible graphene films by hydrohalic acids, Carbon, 48 (2010) 4466-4474.
[45] G. He, H. Chen, J. Zhu, F. Bei, X. Sun, X. Wang, Synthesis and characterization of graphene paper with controllable properties via chemical reduction, Journal of Materials Chemistry, 21 (2011).
[46] D.V.K. Daniela C. Marcano, † Jacob M. Berlin, Alexander Sinitskii, Zhengzong Sun, Alexander Slesarev, Lawrence B. Alemany, Wei Lu, and James M. Tour, Improved Synthesis ofGraphene Oxide, ACS Nano, 4 (2010) 4806-4814.
[47] J. Zhao, W. Ren, H.-M. Cheng, Graphene sponge for efficient and repeatable adsorption and desorption of water contaminations, Journal of Materials Chemistry, 22 (2012).
[48] D. Chen, L. Li, L. Guo, An environment-friendly preparation of reduced graphene oxide nanosheets via amino acid, Nanotechnology, 22 (2011) 325601.
[49] Z. Ying, J. Diao, S. Wang, X. Cai, Y. Cai, H. Liu, N. Wang, Thermal stability, ripening dynamics and coalescing microstructures of reduced graphene oxide-based platinum nanocatalysts: An in-situ TEM study, Diamond and Related Materials, 120 (2021).
[50] I. Bychko, A. Abakumov, O. Didenko, M. Chen, J. Tang, P. Strizhak, Differences in the structure and functionalities of graphene oxide and reduced graphene oxide obtained from graphite with various degrees of graphitization, J Phys Chem Solids, 164 (2022).
[51] W.-T. Chen, R. Muruganantham, W.-R. Liu, Construction of 3D porous graphene aerogel wrapped silicon composite as anode materials for high-efficient lithium-ion storage, Surface and Coatings Technology, 434 (2022).
[52] R. Luo, Z. Li, X. Wu, H. Liu, L. Ma, J. Wu, G. Qin, J. Wang, S. Yang, Super durable graphene aerogel inspired by deep-sea glass sponge skeleton, Carbon, 191 (2022) 153-163.
[53] Y. Song, H. Li, Y. Gao, Q. Yue, B. Gao, W. Kong, Y. Zang, W. Jiang, Grass-modified graphene aerogel for effective oil-water separation, Process Safety and Environmental Protection, 129 (2019) 119-129.
[54] Q. Liu, L. Zhang, H. Chen, J. Jin, N. Wang, Y. Wang, D. Sui, Sulfur and nitrogen co-doped three-dimensional graphene aerogels for high-performance supercapacitors: A head to head vertical bicyclic molecule both as pillaring agent and dopant, Appl Surf Sci, 565 (2021).
[55] J. Xiao, Y. Tan, Y. Song, Q. Zheng, A flyweight and superelastic graphene aerogel as a high-capacity adsorbent and highly sensitive pressure sensor, Journal of Materials Chemistry A, 6 (2018) 9074-9080.
[56] Z. He, W. Chen, B. Liang, C. Liu, L. Yang, D. Lu, Z. Mo, H. Zhu, Z. Tang, X. Gui, Capacitive Pressure Sensor with High Sensitivity and Fast Response to Dynamic Interaction Based on Graphene and Porous Nylon Networks, ACS Appl Mater Interfaces, 10 (2018) 12816-12823.

[57] G. Gilanizadehdizaj, K.C. Aw, J. Stringer, D. Bhattacharyya, Facile fabrication of flexible piezo-resistive pressure sensor array using reduced graphene oxide foam and silicone elastomer, Sensors and Actuators A: Physical, 340 (2022).
[58] W. Yao, R. Mao, W. Gao, W. Chen, Z. Xu, C. Gao, Piezoresistive effect of superelastic graphene aerogel spheres, Carbon, 158 (2020) 418-425.
[59] C. Long, X. Xie, J. Fu, Q. Wang, H. Guo, W. Zeng, N. Wei, S. Wang, Y. Xiong, Supercapacitive brophene-graphene aerogel as elastic-electrochemical dielectric layer for sensitive pressure sensors, J Colloid Interface Sci, 601 (2021) 355-364.
[60] S. Sang, Z. Jing, Y. Cheng, C. Ji, Q. Zhang, X. Dong, Graphene and MXene-based Sponge Pressure Sensor Array for Rectal Model Pressure Detection, Macromolecular Materials and Engineering, 306 (2021).
[61] R. Wang, Z. Tan, W. Zhong, K. Liu, M. Li, Y. Chen, W. Wang, D. Wang, Polypyrrole (PPy) attached on porous conductive sponge derived from carbonized graphene oxide coated polyurethane (PU) and its application in pressure sensor, Composites Communications, 22 (2020).
[62] Y. Xiong, Y. Zhu, X. Liu, P. Zhu, Y. Hu, R. Sun, C.-P. Wong, A flexible pressure sensor based on melamine foam capped by copper nanowires and reduced graphene oxide, Mater Today Commun, 24 (2020).
[63] H.B. Yao, J. Ge, C.F. Wang, X. Wang, W. Hu, Z.J. Zheng, Y. Ni, S.H. Yu, A flexible and highly pressure-sensitive graphene-polyurethane sponge based on fractured microstructure design, Adv Mater, 25 (2013) 6692-6698.